euspen's 22nd International Conference & Exhibition, Geneva, CH, May/June 2022

www.euspen.eu

Development of machine tool spindle with active spindle center position control

Motoki Okabe[1)], Yuya Akiho[1)], Masayuki Obata[2)], Akio Hayashi[1)], Yoshitaka Morimoto[1)]

[1]*Kanazawa Institute of Technology,* [2]*Komatsu NTC Ltd.*

C6100225@planet.kanazawa-it.ac.jp

Abstract

Innovative development of EV have been required for global warming countermeasures. In order to overcome the problem, one of the most efficient method is to realize a non-axisymmetric non-circular inner bore machining within several tens of micrometres. However, there is no machine tool coping with the machining method. Our research purpose is to develop the high-performance spindle that can machine parts by positioning the tool cutting edge to the arbitrary position with electromagnetic force. This developed spindle enable to machine both the inner cylinder profiles for EV motors and internal combustion engines with high precision. The positioning control method has been developed by applying a disturbance observer for the cutting force. Finally, we installed this method into a machining center and evaluated the machining performance of the disturbance observer. From the results of machining experiments, the deviation between the designed input and displacement of tool cutting edge converged into +-1.5 micro meter.

Position control, Bearingless motor, Radial force, Non-axisymmetric surface boring

1. Introduction

In this research, we have developed a new spindle motor that can control both the radial force and the rotational torque simultaneously and synchronously. This makes it possible to control the rotational motion of the spindle and the 2-dimensional position of the tool position attached on the spindle depending on the rotational position simultaneously. Therefore, we have developed a high-performance machine tool spindle based on this concept and aim to machine the non-circular shape as shown in Figure 1. In order to realize this complex surface machining, a control model required for position control of the tool cutting edge of the spindle is constructed. In order to improve the control performance, it is necessary to estimate and eliminate the disturbance due to cutting force. Therefore, we are developing a new control system that can eliminate the actual disturbance estimated by the disturbance observer and feedback the estimated cutting force. By implementing this method on machine tools, the disturbance can be removed accurately and the machined profiles can be expected to obtain the higher accuracy. Also, in the simulation, the performance of the positioning control was evaluated by applying a disturbance assuming the cutting force actually applied. Finally, the performance of the disturbance observer using the actual spindle are evaluated. When a cutting force applied to the actual spindle, the disturbance accurately estimated and eliminated, and the validity of the control model was enough effective for the control.

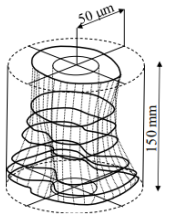

Figure 1. Diagram of non-circular processing

2. Proposed Spindle

Figure 2 shows a schematic diagram of the new spindle unit developed in this study. The spindle motor that has two functions of both a magnetic bearing and AC motor is applied. This motor generates rotational torque and the radial force supporting the spindle with a non-contact manner by the magnetic bearing function. This motor is often called bearing-less motor [1], [2], and can change the radial position by controlling the radial force and rotational position at the same time. As a result, the position of the tool cutting edge can be controlled synchronizing with the spindle rotational position, and the desired cutting edge trajectory can be controlled. The target control stroke is about 5 [μm]. Rated output of bearing-less motor is designed 4.5 kW.

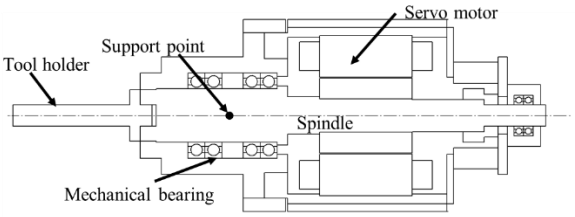

Figure 2. A schematic diagram of the new spindle unit

3. Construction of spindle displacement control model

In this study, the radial motion of the spindle is assumed to be a model of one degree of freedom system. In this case, the equation of motion can be expressed as eq. (1), eq. (2) using the equivalent mass m[kg], damping coefficient c [N/(m/s)], spring constant k[N/m], and radial electromagnetic force f_x. The radial electromagnetic force f_x is proportional to the target position depending on the spindle rotation position. Therefore, the equation of motion is expressed as eq. (3), eq. (4) using the calibration coefficient K_c between force and displacement.

$$f_x = K_c x_{1t}(t) = K_c R\big(\theta(t)\big)\cos(\theta\,(t)) \quad (1)$$
$$f_y = K_c y_{1t}(t) = K_c R\big(\theta(t)\big)\sin\big(\theta(t)\big) \quad (2)$$
$$m\ddot{x}_1\,(t) + c_x\dot{x}_1(t) + k_x x(t) = f_x(t) \quad (3)$$
$$m\ddot{y}_1\,(t) + c_y\dot{y}_1(t) + k_y y(t) = f_y(t) \quad (4)$$

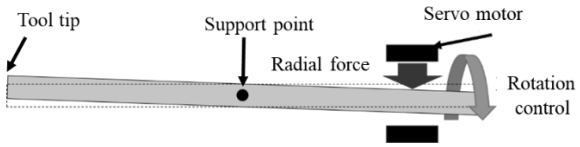

Figure 3. Simple model of spindle

In actual control, in order to keep the control cycle constant, the target position changes depending on the rotation position is obtained synchronizing with the control cycle. Therefore, it is necessary to interpolate the number of data per circumference of the cross section of the workpiece and the data between the rotation positions. Although only the X-axis directional position is described here, the Y-axis directional position can be considered in the same way.

4. Confirmation of transfer function

The main position control of the spindle axis is controlled with a P-I-P position control system as shown in Figure 4. When the step command value of 5 μm is given to the positive direction of the X-axis, the displacement, the velocity from each displacement and the current for supporting force are measured. The transfer function is calculated from these. Figure 5 shows the amplitude of the transfer function. From the figure, although the resonance frequency of the spindle can be confirmed, it is enough small that is not a serious problem for the boring. Therefore, we construct a control model consisting of mass, damping constant, and spring constant from the measured data.

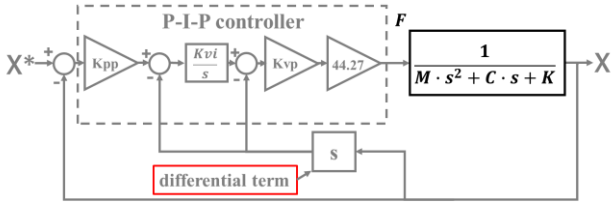

Figure 4. Block diagram for axial center position control

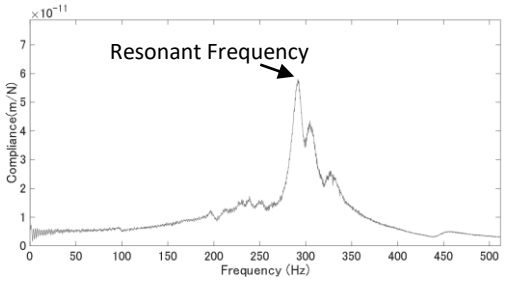

Figure 5. Amplitude of transfer function

5. Parameter estimation

The equivalent mass m [kg], spring constant k [N/m], and damping coefficient c [N/(m/s)] in both X- and Y-axis directions are identified. These are used for control the position of the mass-spring-damper system. The static rigidity was measured by pulling the front end of the prototype with a force gauge. In addition, hammering test was performed on the front end of the rotating shaft of the prototype to measure the dynamic rigidity.

5.1. Identification of spring constant

Figure 6 shows the measuring method for static stiffness and Figure 7 shows the spindle model. As shown in Figure 6, gap capacitance sensors were attached in the X- and Y-axis directions, and the front end of the rotation axis was pulled to the X- and Y-axis directions. At this time, the tensile force was added in a few seconds, and both the tensile force and displacement were measured. The static rigidity was calculated from the measured tensile force and displacement. Here, as shown in Figure 7, some displacement occurs with reference to the fulcrum between the two angular bearings. Therefore, the displacement at the observation point with respect to the radial load was converted into the displacement at the control point and plotted in each of the X- and Y-axis directions. Figure 8 shows the relationship between the tensile force in the X-axis direction and the displacement. The slope of a line in the graph expressed a spring constant obtained dividing the force by the displacement. Based on this, the spring constants in each of the X- and Y-axis directions were identified according to the actual displacement from the experimental procedure.

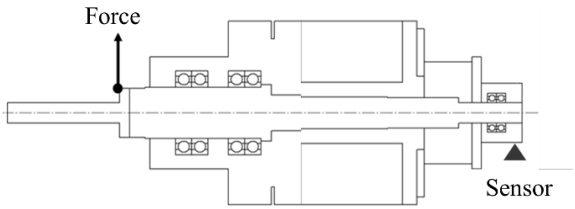

Figure 6. Measuring method of static stiffness

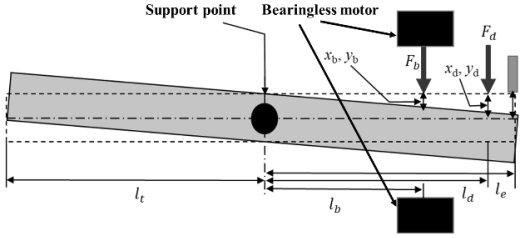

Figure 7. Spindle mode

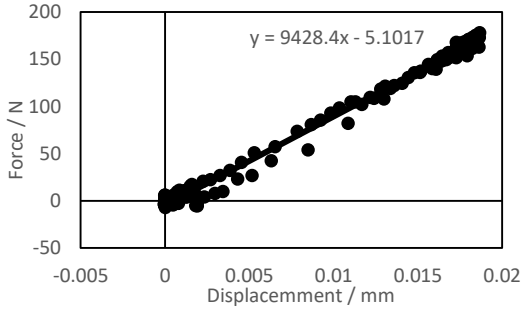

Figure 8. Identification of static rigidity (*X-axis direction*)

5.2. Identification of equivalent mass

Using the obtained resonance frequency and spring constant, the equivalent mass in the radial direction was identified. As shown in Figure 9, a laser displacement sensor was attached to the front end of the rotating shaft of the prototype. The dynamic rigidity was measured by hammering the front end of the rotating shaft in X- and Y-axis directions. Figure 10 shows the

hammering waveform at the tip of the spindle in X-axis direction near the resonance frequency. From the results in Figure 10, it can be seen that the peak frequency in X-axis direction is 275 Hz. Therefore, this frequency was used as the resonance frequency, and the equivalent mass was identified in X- and Y-axis directions. Equations (5) and (6) for identifying the equivalent mass using the spring constant from the difinition of resonance frequency are shown.

$$f = \frac{1}{2\pi}\sqrt{\frac{k}{m}} \tag{5}$$

$$m = \frac{k}{(2\pi f)^2} \tag{6}$$

5.3. Identification of damping coefficient

The logarithmic decrement was calculated from the results of the hammering test that was vibrated in X- and Y-axis directions. Figure 11 shows a result of the hammering test of X-axis direction. From the results in Figure 11, the logarithmic decrement was identified from the ratio of the amplitude in the first waveform to the amplitude in the fifth waveform, and the damping coefficient was identified. The damping coefficient in the Y-axis direction was also identified. As a result of identifying the parameters, all the parameters in X- and Y-axis directions are shown in table 1. The reason why the parameter values are different in the X- and Y-axis directions is that the different responses are obtained in each direction depending on the structure that supports the spindle. From these results, the spindle system can be considered as a model of the spring-damper system in X- and Y-axis directions as shown in Figure 12.

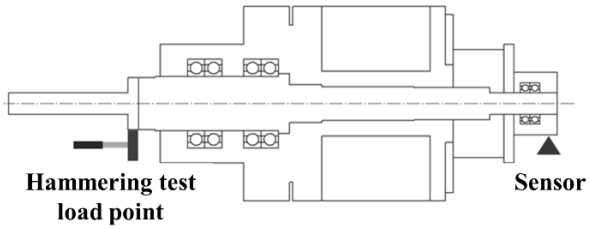

Figure 9. Measuring method of dynamic stiffness

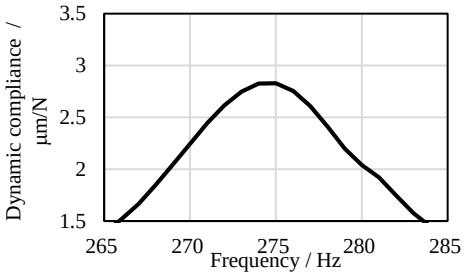

Figure 10. Dynamic rigidity (*X-axis direction*)

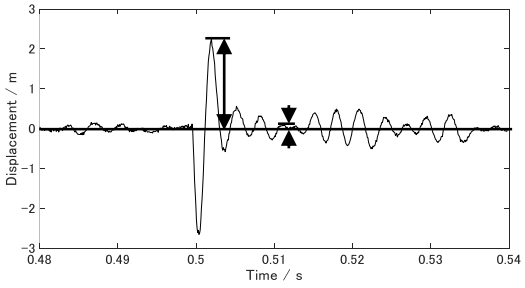

Figure 11. Logarithmic decrement (*X-axis direction*)

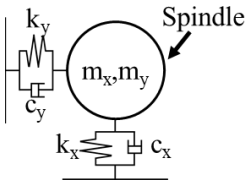

Figure 12. Two-way model of spindle

Table1 Identified model parameters

	Equivalent mass[kg]	Spring constant[N/m]	Damping coefficient[N/(m/s)]
x	4.723	1.41e7	1340.643
y	4.594	1.17e7	2233.628

6. Building up a disturbance observer

A control model with a disturbance observer is build up and implemented. Figure 13 shows a block diagram that includes control of the magnetic force of the spindle by attaching a P-I-P controller. All the parameters are shown in table 2. A simulation was performed to remove disturbances, assuming an actual testing machine. The command value is converted into force by the P-I-P controller and the conversion coefficient of current and force. After that, the disturbance estimates obtained by the disturbance observer were fed back to suppress the disturbance.

In addition, the input was set to 0 [m] and the state was made stationary, and a ramp-like disturbance (a disturbance that became 0 to 10 [N] in 0.05 seconds) was added assuming actual boring processing. A simulation was performed under these conditions to confirm the disturbance removal effect with and without the disturbance observer. Figure 14 shows the added disturbance. Sampling frequency is 12.5[kHz]. The cutoff frequency of the low-pass filter is 1 [kHz].

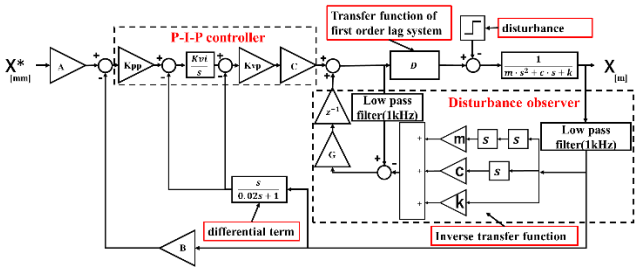

Figure 13. Block diagram with disturbance observer

Table2 Experimental parameters

m[kg]	4.723	A(Unit conversion coefficient)	10
c[N/(m/s)]	1340.643	B(Unit conversion coefficient)	10000
k[N/m]	14100000	C(Current-force conversion factor)[A/N]	44.27
K_{pp}	0.2	D(Transfer function of first order lag system)	$\frac{4341s + 556900}{s^2 + 6053s + 556600}$
K_{vi}	150		
K_{vp}	400	G(Observer control gain)	0.5

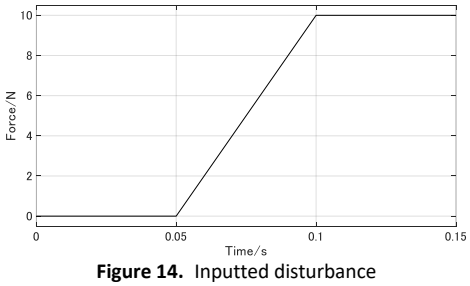

Figure 14. Inputted disturbance

7. Verification of disturbance removal effect

7.1. About the disturbance removal effect by simulation

Figures 15 show the results without and with the disturbance observer when the disturbance becomes constant in 0.05 seconds. It can be seen that it takes time to converge without feedback, whereas the waveform converges quickly with feedback. In the case of without feedback, the minimum output value became smaller and the amplitude reduction rate was 66.3%. The result demonstrates that our control system was able to estimate the disturbance and accurately remove the added disturbance.

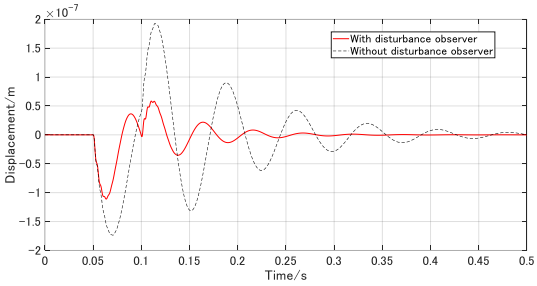

Figure 15. Output displacement

7.2. About the disturbance removal effect by machining test

The effectiveness of the disturbance observer was verified by machining test. For the rotation trajectory, the origin support control was used to set the axis center at x and y to 0 positions.

Figure 16 shows the output without the disturbance observer, Figure 17 shows the output with the disturbance observer, Figure 18 shows the observer calculation result. Comparing the displacements in the X- and Y-axis directions, it can be seen that the result with the disturbance observer is about 30% closer to the origin than the one without it in both the X- and Y-axis directions. Figure 19 shows the comparison of both with and without disturbance observer.

The origin support performance was better with the disturbance observer, indicating that the disturbance observer functioned effectively.

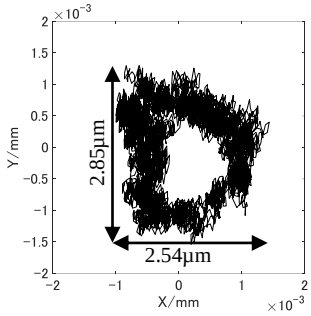

Figure 16. Displacement without disturbance observer

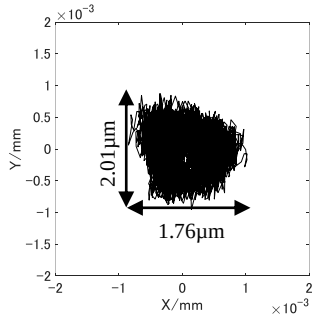

Figure 17. Displacement with disturbance observer

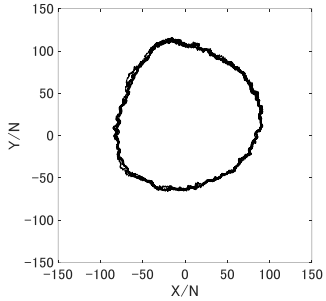

Figure 18. Observer calculation result

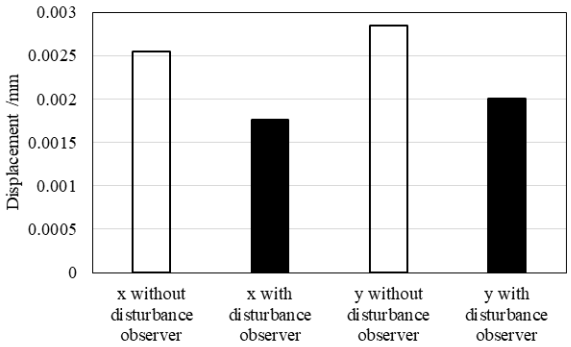

Figure 19. Compared result of both with and without disturbance observer

8. *Conclusions*

In this study, we have developed a new machine tool spindle with a special motor that can control the radial force and the rotational torque simulatiously and synchronizing. The results obtained were as follows:

1) The coefficients of spring constant, equivalent mass, and damping force used in the spring-damper control model were identified.

2) A disturbance observer that can estimate and remove the disturbance of the spindle was developed.

3) It was confirmed by simulation that the proposed disturbance observer can estimate and remove disturbances effectively.

4) Through machining tests, it was confirmed that the disturbance observer was effective for control performance.

Further developments are planned to machine the inner boring for the EV motor case and the inner combustion cylinder by installing this spindle into the machining center.

Acknowledgement

This work was supported by JSPS KAKENHI 20K04215. We would like to express our gratitude for this support.

References

[1] Syunsuke Kobayashi, Masahide Ooshima, A Radial *Position Control Method of Bearingless Motor Based on d–q-Axis Current Control*, IEEE Transactions on Industry Applications vol.**49** No4, (2013), pp.1827-1835.

[2] Masahide Ooshima, *"Stabilized Control Strategy under Loaded Condition at Failure of a Motor Section in a d-q Axis Current Control Bearingless Motor", IEEE Power and Energy Society 2017 General Meeting, Panel Session, 17PESGM2558, (2017).*

[3] Yuya AKIHO, Masayuki OBATA, Motoki OKABE, Akio HAYASHI, Yoshitaka MORIMOTO, *"Active center position control of machine tool spindle"*, JSME Leading Edge Manufacturing in 21st Century (LEM21),(2021)